Cancer Imaging (2013) **13(1),** 81–91
DOI: 10.1102/1470-7330.2013.0009

REVIEW

Dual-energy CT imaging of thoracic malignancies

Long Jiang Zhang[a,1], Gui Fen Yang[b,1], Sheng Yong Wu[c], Jian Xu[a], Guang Ming Lu[a], U. Joseph Schoepf[d]

[a]Department of Medical Imaging, Jinling Hospital, Clinical School of Medical College, Nanjing University, 305 Zhongshan East Road, Xuanwu District, Nanjing, Jiangsu Province, 210002, China; [b]Department of Nuclear Medicine, Jinling Hospital, Clinical School of Medical College, Nanjing University, China; [c]Tianjin Medical Imaging Institute, Tianjin, 300192, China; [d]Department of Radiology and Radiological Science, Medical University of South Carolina, Charleston, SC, USA

Corresponding address: Jian Xu or Guang Ming Lu, Department of Medical Imaging, Jinling Hospital, Clinical School of Medical College, Nanjing University, Zhongshan East Road 305, Xuanwu District, Nanjing, Jiangsu Province, 210002, China.
Email: 13851656307@163.com; cjr.luguangming@vip.163.com

[1]Long Jiang Zhang and Gui Fen Yang contributed equally to this work.

Date accepted for publication 19 December 2012

Abstract

Computed tomography (CT) plays a pivotal role in the detection, characterization, and staging of lung cancer and other thoracic malignancies. Since the introduction of clinically viable dual-energy CT techniques, substantial evidence has accumulated on the use of this modality for imaging chest malignancies. This article describes the principles of dual-energy CT along with suitable image acquisition, reconstruction, and postprocessing strategies for oncologic applications in the chest. The potential of dual-energy CT techniques for the detection, characterization, staging, and surveillance of chest malignancy, as well as the limitations of this modality are discussed.

Keywords: *Lung cancer; dual energy; dual source; X-ray computed tomography.*

Introduction

Lung cancer is one of the most common malignancies worldwide and is the leading cause of cancer death in the United States among both men and women, with an estimated 222,520 new cases and 157,300 deaths every year, which constitutes approximately 28% of all cancer deaths[1]. Despite all efforts, lung cancer remains a challenging disease to effectively identify, diagnose, and treat. Its 5-year survival rate remains similar to that of 15 years ago at 13% for all stages (clinical staging)[2]. Thus, it is imperative to develop new algorithms and techniques for the characterization of lung nodules and staging of lung cancer. Although many imaging techniques, such as computed tomography (CT), magnetic resonance imaging (MRI), and positron emission tomography (PET)/CT, have been used in the detection, characterization, and follow-up of lung cancer, CT remains the mainstay modality in this arena because of its high-resolution anatomic imaging capabilities. However, newer, versatile CT techniques have been described that make use of lesion enhancement to image angiogenesis and other imaging markers of disease activity. Dual-energy CT (DECT) techniques based on either dual-source CT systems or single-source CT with rapid kilovoltage switching, take advantage of the material differentiation of iodine, and simultaneously provide virtual non-contrast medium-enhanced and iodine-enhanced image series from a single contrast-enhanced scan[3,4]. Although the understanding and usage of DECT in the thoracic oncology realm is at the very early stages, substantial evidence has accumulated on the potential of DECT for imaging a vast variety of chest diseases, including lung nodules and lung cancer. This article reviews the technical principles of DECT along with suitable imaging strategies in the context of chest malignancy as well as the limitations of this modality.

DECT systems

The introduction of dual-source CT in 2005 ushered in the availability of clinically viable, robust and relevant DECT applications. Since then, the clinical use of DECT has been increasing as more and more radiologists become familiar with this technique and its inherent benefits.

Briefly, DECT imaging is based on the differential attenuation of tissues when penetrated with higher (140 kVp) and lower (80/100 kVp) energy photons[5,6]. The underlying physical principles of DECT imaging have been reviewed in great detail in several other excellent contributions published elsewhere[7,8].

Currently, clinically available CT systems capable of DECT applications include dual-source, dual-energy CT (dsDECT) and single-source DECT (ssDECT) with fast kVp switching. To date, the majority of clinical experience has been accumulated using dsDECT techniques.

The dual-source CT system is composed of two X-ray tubes and two corresponding detectors (Fig. 1A). The two acquisition systems are mounted on the rotating gantry with an angular offset of 90° (first generation dual-source CT) or 95° (second generation dual-source CT). For DECT acquisitions, the tube voltage is set at high energy (140 kVp) for one tube and at lower energy (80 or 100 kVp) for the other tube. The tubes rotate simultaneously in a fixed position relative to each other, thus avoiding temporal differences in projection sampling. Because of detector size differences, the fields of view of the tubes are 50 cm and 26 cm (first generation) and 33 cm (second generation), respectively. In second generation dual-source CT scanners, an Sn (tin)-based photon shield filters lower-energy photons from the 140-kVp beam to provide better separation of photon energies between the two X-ray beams, improving the ability of material decomposition[5–7].

The fast kilovoltage switching technique uses a single X-ray source (Fig. 1B). A generator rapidly alternates the tube energies from low energy (80 kVp) to high energy (140 kVp) to acquire DECT data with very small temporal differences[5]. In contrast to dsDECT, the field of view of ssDECT is 50 cm for both high-kVp and low-kVp data. Image analysis for ssDECT is performed on projection data, while dsDECT is based in the image domain. However, with ssDECT, the tube current cannot be changed while simultaneously switching the tube potential; thus, automated tube current modulation for reducing radiation exposure is not available with ssDECT techniques[4].

Single-source CT systems with layered detector materials are under development, but are not yet available for routine clinical use. With this approach, the detector comprises two layers, an upper layer that absorbs the lower-energy photons and a lower layer registering the remaining higher-energy emissions. From these two datasets, two separate image series are reconstructed and analyzed[6]. The data acquisition procedure is similar to the standard single-energy CT scan and a full field of view (50 cm) is available. The advantage of this DECT approach is matching temporal and spatial domains for low-energy and high-energy CT data sets; its main limitation is the potential marked spectral overlap between low-energy and high-energy CT data[4].

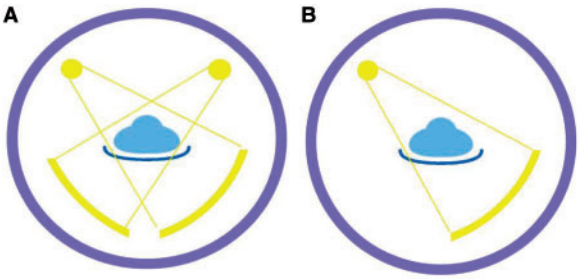

Figure 1 **Configuration of currently available CT scanners capable of dual-energy acquisition. (A) Dual-source CT; (B) single-source CT with fast kVp switching.**

Image reconstruction and postprocessing

Processing of DECT data is done in the image domain or in the data domain. With dsDECT, the raw spiral projection data of both tubes are automatically reconstructed into three separate image series: Selective low-energy (80/100 kVp) and high-energy (140 kVp) series, and an average weighted series equivalent to a 120-kVp image acquisition. Images at 80 kVp have higher contrast and improve lesion visualization but are associated with higher image noise, whereas 140-kVp images have lower contrast and noise and contribute finer anatomic detail and edge delineation. At our institutions, we use a low/high kVp linear weighting of 0.3 (i.e., 30% image information from the lower kVp image series and 70% information from the 140-kVp series) to reconstruct average weighted 120-kVp images. However, linear weighting of 0.5 or 0.6 has also been recommended in some published studies[9,10]. For each image set, we uniformly use a section thickness of 0.75 mm and a reconstruction increment of 0.50 mm at our institutions.

Virtual non-contrast images and iodine images

Using the DECT technique, it is possible to differentiate iodine from other high-attenuation materials by the material decomposition theory to provide material-specific images (virtual non-contrast images and iodine-enhanced images) and energy-specific images (monochromatic images). With dsDECT scanners, virtual non-contrast (VNC) images for oncologic chest applications are preferentially obtained using the lung nodule (Fig. 2A)

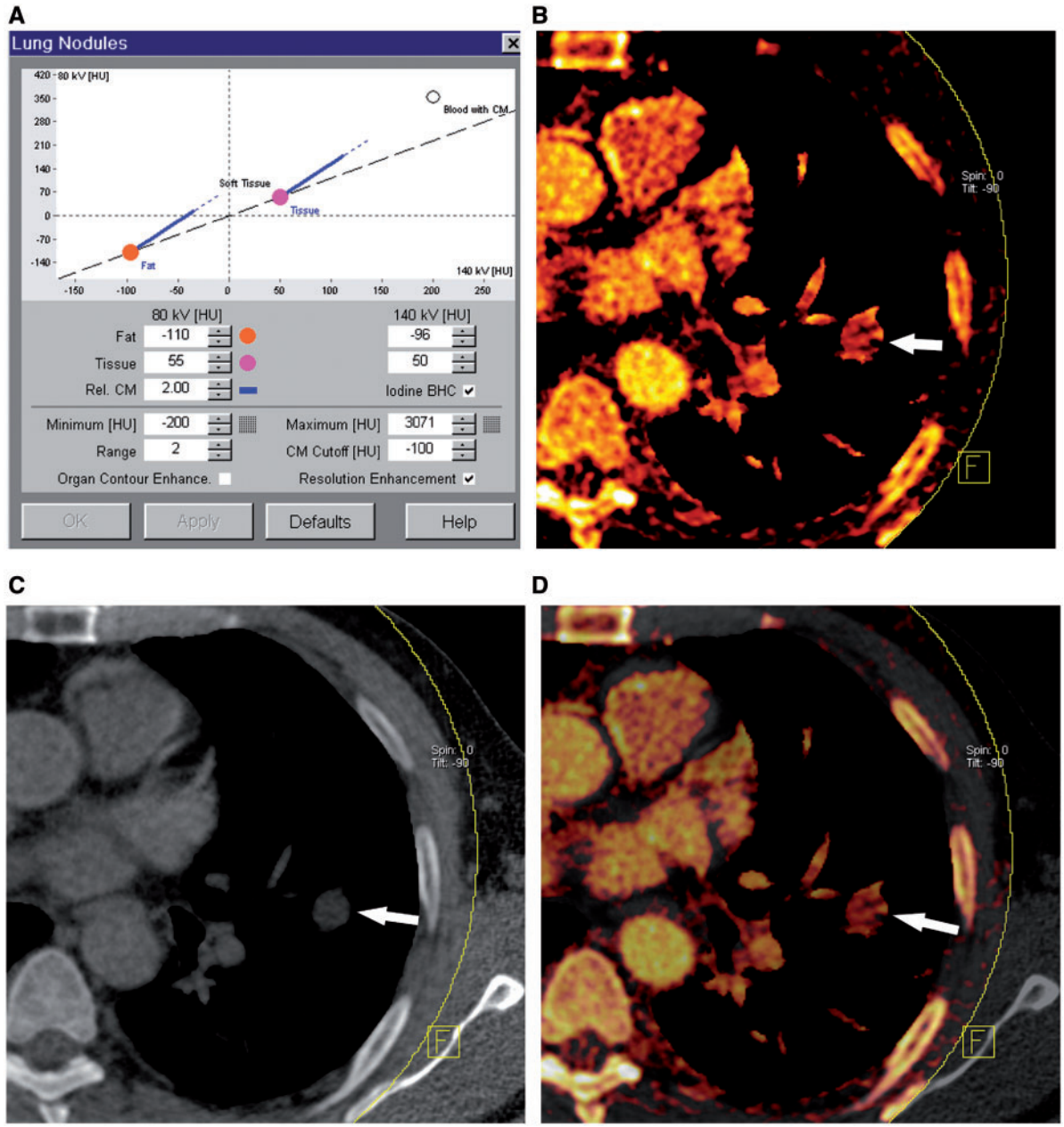

Figure 2 **Lung nodule application. (A) Lung nodule application software interface. The left column shows reference attenuation values at 80 kVp: −110 HU for fat and 55 HU for soft tissue. The right column shows these values at 140 kVp: −96 HU for fat and 50 HU for soft tissue. Relative contrast material enhancement (rel. CM) at 80 kVp compared with that at 140 kVp is 2.0. In this mode, the software calculates the iodine distribution only in soft tissue between −200 HU and 3071 HU; contrast material cutoff is set at −100 HU, and 2 for range. The range refers to the number of adjacent voxels used for interpolation during the calculation of the three-material decomposition, with smaller values yielding higher spatial resolution and larger values improving detection of small contrast differences. (B) Iodine map shows the enhanced lung nodule (arrow) in the left lower lobe. (C) VNC image shows the nodule without calcification (arrow). (D) Iodine overlay image shows the enhancement of the lung nodule (arrow) and related anatomic details.**

application with the three-material decomposition algorithm[11]. With this application, three image sets can be obtained: one image series displays the Hounsfield unit value due to iodine attenuation (iodine image) (Fig. 2B); the other series displays the Hounsfield unit value due to remaining body materials (VNC image) (Fig. 2C). Fused images display the iodine enhancement overlaying the anatomic image (Fig. 2D). With ssDECT, two-material decomposition is performed, which uses linear attenuation coefficients[4]. In ssDECT, appropriate base materials, such as iodine and water, should be selected. The iodine/water base material pair is commonly used for

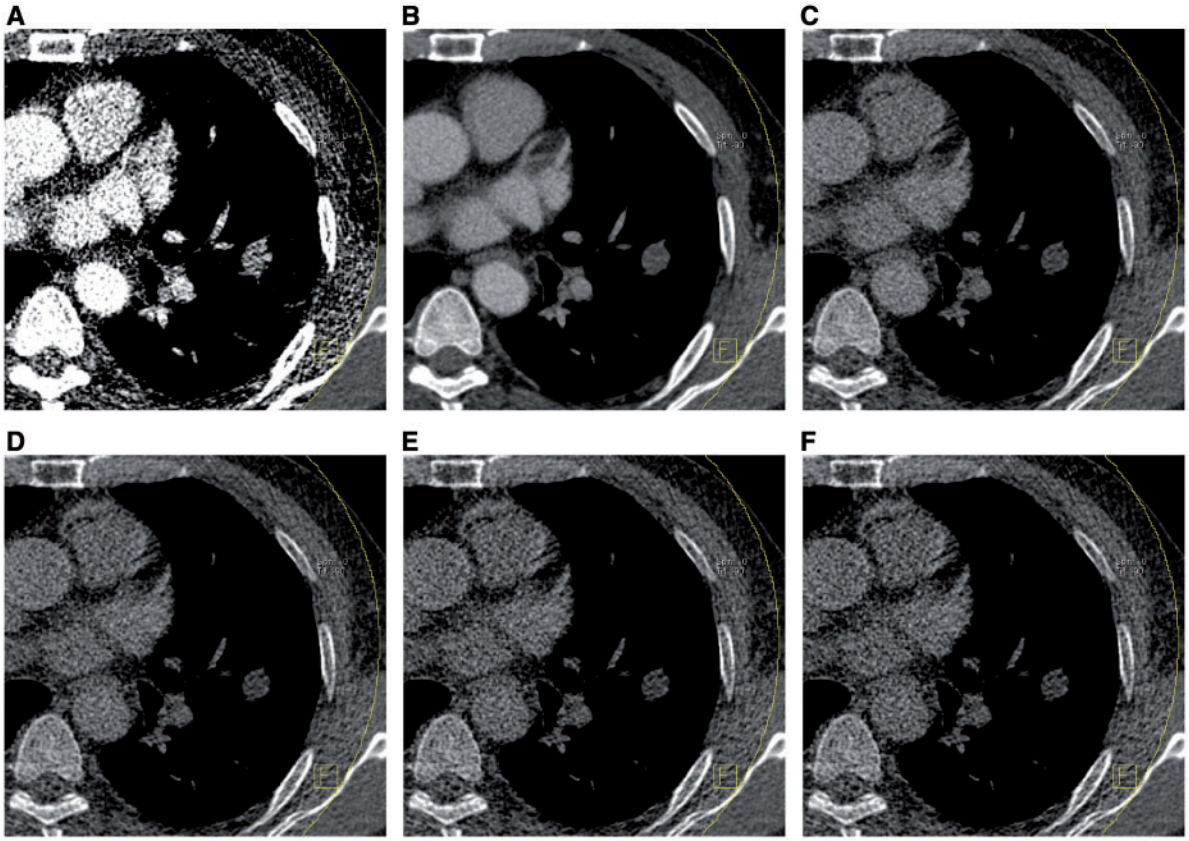

Figure 3 **Monochromatic monoenergetic images in a 62-year-old man with lung cancer. (A) 40 keV; (B) 70 keV; (C) 100 keV; (D) 130 keV; (E) 160 keV; (F) 190 keV; These monochromatic images were obtained using the first-generation dual-source CT scanner. Reconstruction of image series at the 70-keV energy level shows the best compromise between image noise and contrast resolution.**

abdominal imaging; this generates an iodine density image and a water density image[12]. The water density image does not have any image voxels with attenuation similar to iodine, and hence serves as a virtual unenhanced image[12].

VNC images can provide information equivalent to a true non-contrast medium enhanced image and hence can be used to substitute for a true unenhanced scan, thus reducing the radiation dose to the patient for the whole CT examination[11]. Iodine images or iodine overlay images can be used to measure enhancement within the lesion or target tissue, which is expressed in Hounsfield units (HU) with dsDECT and milligrams per milliliter (mg/ml) with ssDECT.

Monochromatic images

Monochromatic monenergetic images can be generated based on DECT techniques that analyze projection (raw) data and image data. These images are generally called monochromatic images although a more accurate description would be virtual monochromatic images as they are generated by calculating energy-selective monochromatic projections from the dual-energy data and not from a true monochromatic X-ray source[3]. Using projection data, curves of CT numbers of different materials can be displayed over a range of 101 energies (40–140 keV)[3]. When using image data, a range of 40–190 keV can be used[13] (Fig. 3). Although monochromatic images can be reconstructed at any keV levels between 40 and 190 keV, images reconstructed between 65 and 75 keV have less noise and a higher contrast-to-noise ratio[3] (Fig. 3). Potential applications of monochromatic, monenergetic techniques have been reported for the assessment of thyroid nodules, liver lesions, renal stones, and implanted metal devices (to reduce beam hardening artifacts)[3–5,12–14].

Characterization of lung nodules

The most common initial manifestation of lung cancer is a solitary pulmonary nodule (SPN) smaller than 3 cm in diameter[15]. Diagnostic evaluation of SPNs is highly relevant because of the frequency and implications of this finding. DECT can simultaneously provide a VNC medium enhanced series and an iodine-enhanced image from a single scan acquisition (Fig. 2C). This quality has proved useful in the further characterization of SPNs by

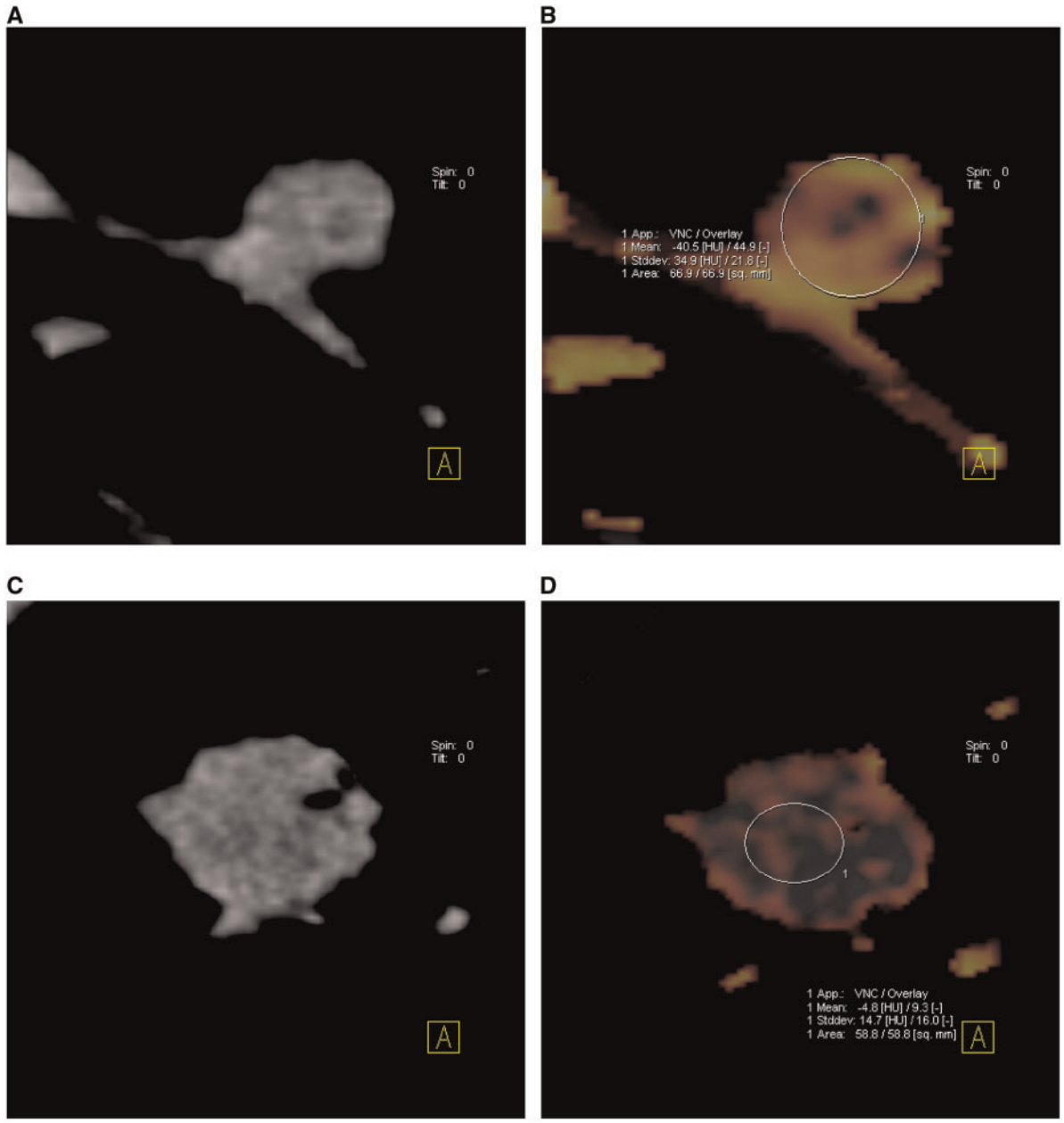

Figure 4 **Quantitative measurements of solitary pulmonary nodules on conventional CT and a DECT iodine map. (A) Contrast-enhanced conventional CT image shows heterogeneous lesion enhancement; (B) DECT iodine map shows lung cancer with a typical avid mean enhancement value of 44.9 HU; (C) contrast-enhanced CT image shows heterogeneous lesion enhancement and air bronchograms; (D) DECT iodine map demonstrates an inflammatory nodule with lower enhancement values (9.3 HU).**

demonstrating iodine-related attenuation and calcification[16–18]. Chae et al.[16] evaluated the clinical utility of DECT for the tissue classification of SPNs. This study included 49 patients with a total of 45 nodules, which were confirmed as benign or malignant on the basis of percutaneous needle aspiration histology. The prevalence of malignancy was 55.6% (25 of 45 nodules). CT numbers on virtual non-enhanced and non-enhanced weighted average image series and CT numbers on the iodine-enhanced series as well as the degree of enhancement showed good agreement. On virtual non-enhanced series, 85.0% (17 of 20) of calcifications in SPNs and 97.8% (44 of 45) of calcifications in lymph nodes were detected, and the apparent sizes were smaller than those on the non-enhanced weighted average series. Radiation dose (average dose × length product, 240.77 mGy cm) was not significantly different from that of single-energy CT ($P = 0.67$). Diagnostic accuracy for malignancy by using CT numbers on iodine-enhanced image series with a cutoff of 20 HU was comparable

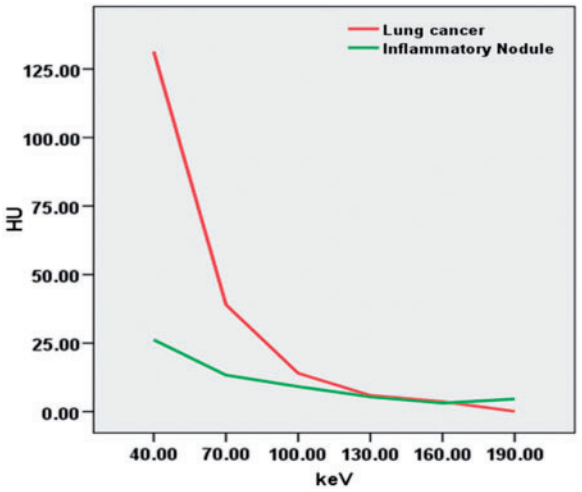

Figure 5 **Spectral curves from two lung nodules. (A) Lung cancer, color coded in red, in a 62-year-old man; (B) inflammatory nodule, color coded in green, in a 28-year-old woman.**

with that using the degree of enhancement (sensitivity, 92% and 72%; specificity, 70% and 70%; accuracy, 82.2% and 71.1%, respectively) (Fig. 4).

Monochromatic monoenergetic imaging may allow characterization of tissues by studying their attenuation to X-rays at consecutive energy levels, which could be advantageous for differentiating tissues that cannot be distinguished with standard CT imaging due to identical attenuation. Thus, this approach may have potential for the differentiation of benign and malignant lung lesions (Fig. 5). No reports on ssDECT for lung nodule evaluation are available to date, and further studies are warranted to clarify the potential role of monochromatic imaging in the characterization of lung nodules.

Ground-glass opacities (GGO) are hazy lung lesions with increased attenuation, with preservation of bronchial and vascular margins[19]. GGOs of the lung are increasingly detected by CT and can represent lung adenocarcinoma, the predominant type of lung cancer today. Conventionally, GGOs are diagnosed morphologically using non-contrast medium enhanced CT. However, GGOs can result from inflammation, hemorrhage, or fibrosis. Attempts to evaluate contrast enhancement of GGOs may be helpful to further characterize such lesions because pathologic studies[20,21] showed increased blood vessel density in adenocarcinoma, including bronchioloalveolar carcinoma, and lesion enhancement is assumed to suggest malignancy. Practically, however, evaluating the contrast enhancement of GGOs is challenging. It is difficult to evaluate the contrast enhancement of GGO visually and their inhomogeneity makes it difficult to place a region of interest on precontrast and postcontrast series without misregistration. Kawai et al.[22] evaluated the feasibility of measuring contrast enhancement of GGO lesions by DECT. Their study enrolled 24 patients with pure GGO or GGO-dominant nodules. Of 24 patients, 23 underwent pulmonary resection, and the lesions were pathologically confirmed; 1 patient was diagnosed as having benign inflammatory change because the lesion shrank markedly in a 4-month follow-up period without any treatment. They found increased iodine-related attenuation in 22 adenocarcinomas but not in pulmonary hemorrhage or inflammatory changes. These authors concluded that DECT may be a useful modality for the characterization of mixed GGO, the type with the highest malignancy rate in this lesion class[23].

Staging of lung cancer

For the staging of lung cancer, the value of DECT lies in the visualization and characterization of hilar and mediastinal lymph nodes, which is helpful for the N staging of lung cancer. Recently, Ogawa et al.[24] reported that DECT studies acquired 60 s after contrast injection showed excellent vessel–lymph node contrast on 80-kVp images because of reduced beam hardening artifacts from the contrast material. Lesion enhancement on weighted average 120-kVp images was shown to serve as a substitute for dual phase scan protocols. For more extensive lung tumors, Schmid-Bindert et al.[17] found moderate correlation between the maximum standard uptake value (SUV_{max}) and the maximum iodine-related attenuation of DECT in all tumors. Analysis of histologic subtypes of lung cancer showed a stronger correlation between SUV_{max} and the maximum iodine-related attenuation in non-small cell lung cancer (NSCLC) than in small cell lung cancer (SCLC), which could be explained by differences in tumor biology such as different angiogenetic features between NSCLC and SCLC. These findings indicate that measurement of the maximum iodine-related attenuation on DECT may be a useful surrogate parameter for the evaluation of therapy response of lung cancer (Fig. 6). However, a lower correlation between SUV_{max} and the maximum iodine-related attenuation in thoracic lymph nodes was noted, possibly because of differences in neoangiogenesis between intrapulmonary tumors and lymph node metastases. The limited accuracy of both imaging tests to differentiate metastatic from reactive inflammatory lymph nodes may be an alternate explanation. Thus, further studies seem warranted to clarify the role of DECT for lymph node staging of lung cancer as there are no established data available that define the role of DECT for this purpose.

Potential future applications in lung cancer

DECT may have potential applications in the pre- and postoperative evaluation of lung cancer. The currently available DECT techniques include iodine-based contrast-enhanced DECT lung perfusion imaging and xenon-enhanced DECT lung ventilation imaging. DECT

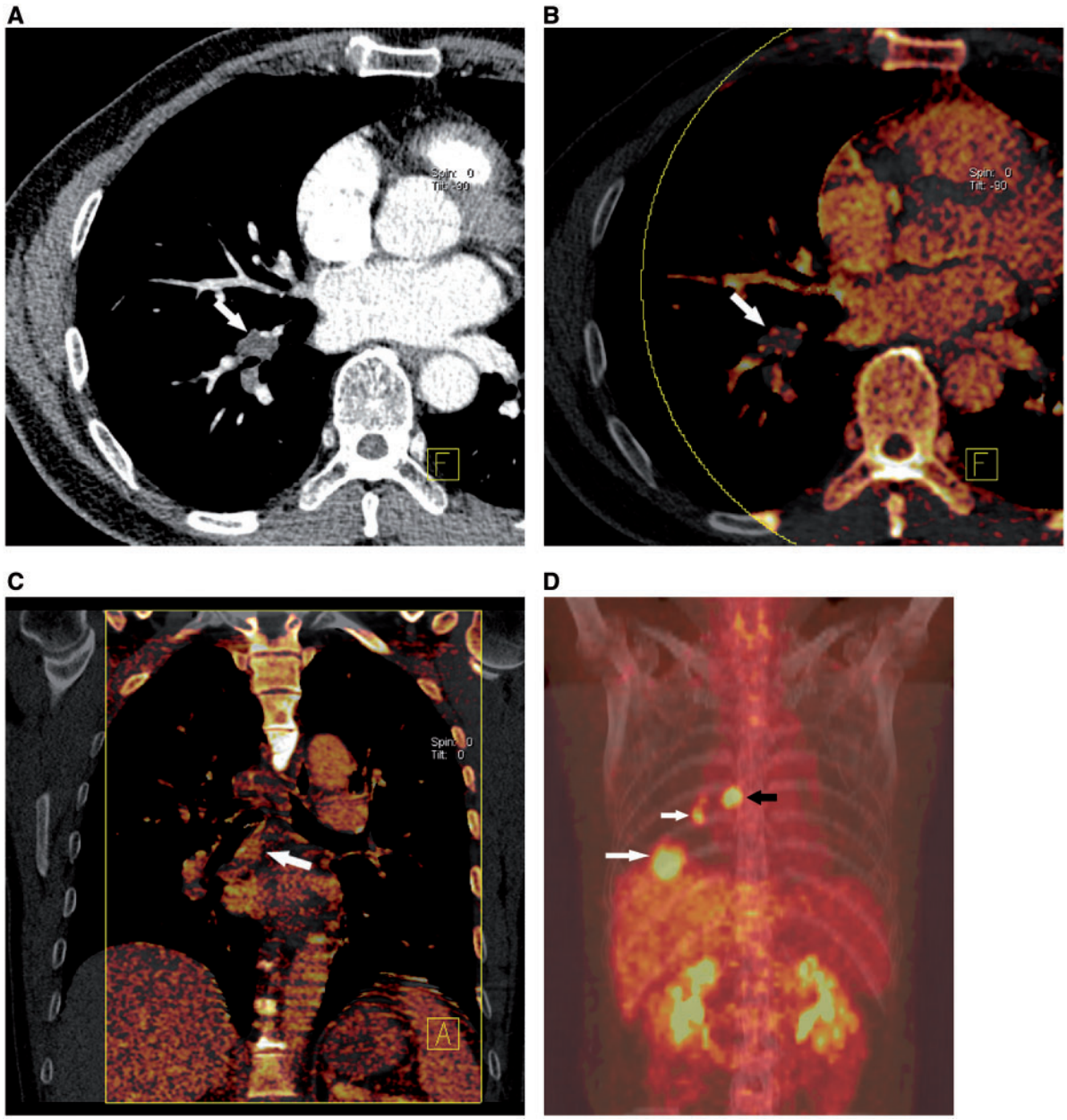

Figure 6 **Mediastinal lymph node in a 52-year-old man with lung cancer. (A) Axial contrast-enhanced CT image acquired at 30 s and (B) axial iodine overlay map acquired at 60 s after intravenous administration of iodinated contrast agent show the enlarged right hilar lymph node (arrow). (C) Coronal iodine overlay image shows the enhanced mediastinal lymph node (arrow). (D) [^{18}F]Fluorodeoxyglucose-positron emission tomography/CT shows the right lower lung mass (long white arrow) and right hilar (short white arrow) and mediastinal (black arrow) lymph nodes with increased fluorodeoxyglucose uptake corresponding to dual-energy CT findings.**

allows analysis of the regional lung perfusion status by demonstrating iodine concentration in the lung parenchyma and vascular obstruction by visualizing intravascular filling defects, which is helpful in the detection and prognosis of pulmonary embolism[25–29]. Accordingly, dsDECT pulmonary angiography has been advocated as a one-stop-shop modality for the acute pulmonary embolism[30].

Xenon-enhanced DECT can be used to map regional lung ventilation function. The atomic number of xenon is 54, which is similar to that of iodine. Thus, this element has X-ray absorption characteristics that resemble those of iodine (i.e., strong attenuation at low kilovoltage)[31] and can thus serve as an inhalation contrast agent for CT ventilation imaging, although this application is not currently approved for clinical use in the United States. With xenon-enhanced DECT, ventilation maps of the lung can be generated to visualize the ventilation function in patients with chronic obstructive pulmonary disease and asthma. Collateral ventilation can also be visualized

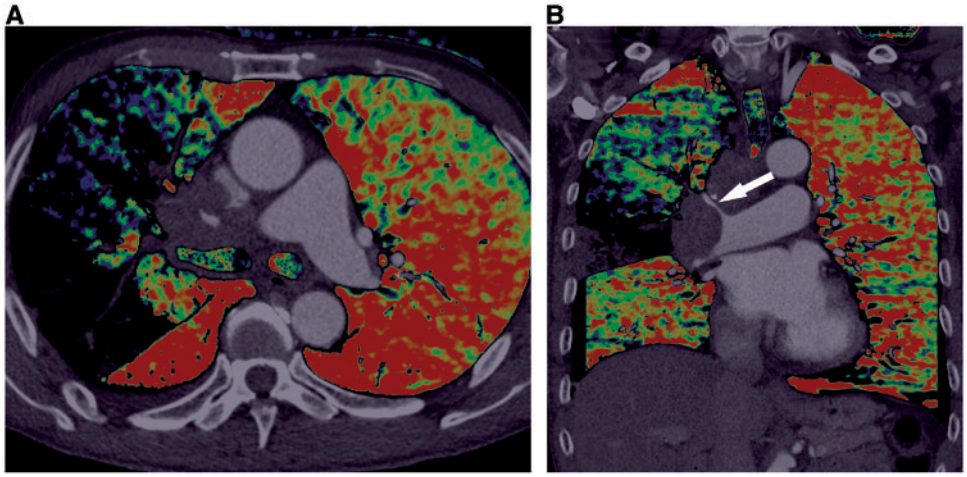

Figure 7 **Blood pool defect in a pulmonary blood volume map caused by lung carcinoma in a 70-year-old man. Dual-source CT-based DECT pulmonary blood pool study. (A) Axial and (B) coronal fused images show a right lung carcinoma invading the hilar vasculature (arrow), resulting in diffuse decreased blood distribution within the right lung.**

with dynamic xenon-enhanced DECT in patients with bronchial atresia or obstruction and congenital hyperlucent lung lesions[32,33]. DECT perfusion and ventilation imaging can be accomplished during the same CT examination, enabling the simultaneous assessment of regional lung perfusion and ventilation from a single scan[34].

In patients with lung cancer, especially central lung cancer, DECT can depict the presence and extent of perfusion (Fig. 7) or ventilation (Fig. 8) defects and collateral ventilation when the mass involves the hilar vessels or bronchi, aiding in the preoperative prediction of postoperative pulmonary perfusion and ventilation function. Preoperative prediction of postoperative pulmonary function is traditionally performed by radionuclide scintigraphy. However, DECT emerges as an attractive one-stop-shop modality for imaging lung cancer, including tumor characterization, staging, and prediction of postoperative pulmonary function. The use of DECT could thus obviate the need for radionuclide scintigraphy for the assessment of lobar perfusion or ventilation status before surgery.

Radiation dose

dsDECT is performed with dynamic tube current modulation (CARE Dose4D) to reduce radiation dose. Thus, dsDECT is radiation-dose neutral compared with similar protocol studies performed with traditional single-energy multidetector-row CT (MDCT) because each tube delivers approximately half of the total radiation dose[18]. This was demonstrated by Chae et al.[16], who showed that the radiation dose of DECT covering the full thorax (240.77 ± 37.18 mGy cm) is similar to that of single-energy MDCT (235.38 ± 35.40 mGy cm) or dual-source CT in single-energy mode (233.13 ± 67.36 mGy cm). Pontana et al.[35] reported a mean dose $\times$ length product of dsDECT-based CT pulmonary angiography of 280 mGy cm, corresponding to an average effective patient dose of about 5 mSv. We previously showed that the effective radiation dose from dsDECT-based CT pulmonary angiography ranged from 1.1 to 7.1 mSv (mean 2.3 ± 1.1 mSv) in the pediatric population[36], which is comparable with that (2–5 mSv) reported by Victoria et al.[37] and lower than that (average 10.5 mSv; range 2.3–26 mSv) reported by Kritsaneepaiboon et al.[38] using single-source, single-energy MDCT pulmonary angiography. Conversely, the radiation dose with ssDECT imaging has been reported to be higher than that of single-energy MDCT, which is attributed to the lack of tube current modulation because of the inability to change the tube current while simultaneously switching the tube potential with ssDECT imaging.

In a routine clinical work flow, however, the ability to derive virtual non-enhanced images based on DECT scanning may replace the additional non-enhanced CT scan, thus reducing the radiation dose to the patient. In addition, the substantial incremental diagnostic gain by use of DECT for lung examinations may obviate the need for additional clinical tests that involve radiation, thus reducing the net exposure of the individual patient.

Use of DECT for extrathoracic applications

A wide variety of extrathoracic DECT applications have been reported, especially in the abdomen. For instance, DECT has been used to analyze renal stone composition[4], obtain vitrtually non-enhanced CT images[3–5,11] in lieu of additional true non-contrast acquisitions, and to characterize renal masses[3–5]. In addition, the use of DECT has been reported for evaluating ischemic heart disease[39,40] and the detection of intracranial hemorrhage[41].

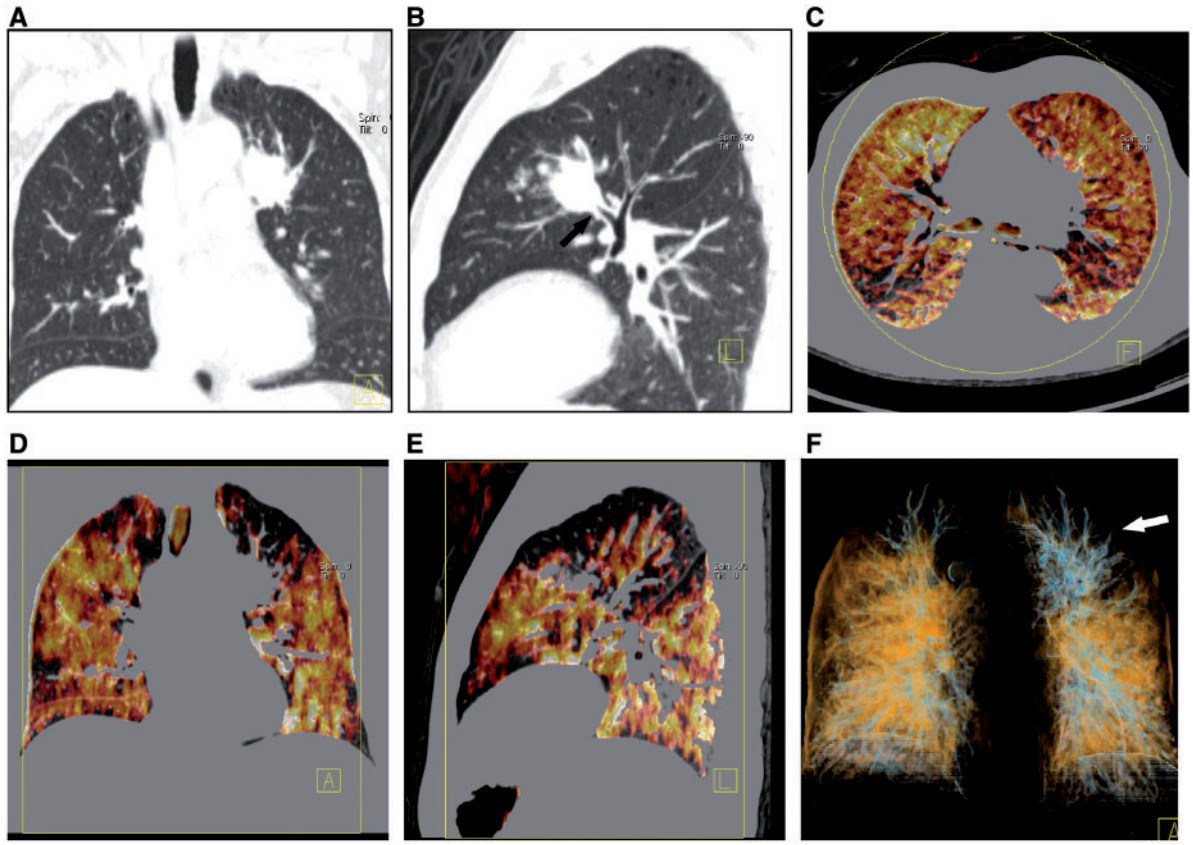

Figure 8 **Xenon-enhanced dual-energy CT lung ventilation study in a 54-year-old man with lung cancer in the left upper lobe. DECT based chest CT acquisition under inhalation of xenon gas. (A) Coronal and (B) sagittal reformatted CT images of lung window show left anterior bronchus obstruction (arrow) by the mass. (C) Axial, (D) coronal, (E) sagittal xenon overlay images, and (F) volume rendering DECT xenon map show the ventilation defect in the upper lobe of the left lung (arrow). Heterogeneous xenon distribution in both lungs is attributed to emphysema in this patient.**

Limitations

DECT provides useful information for lung nodule characterization, lung cancer staging, and preoperative assessment of postoperative lung function by material decomposition. However, these techniques have not been widely used to date in clinical practice as a mainstream oncology application. Some limitations of this technique need to be fully recognized in order to exhaust the full potential of this modality for routine clinical applications. First, DECT technology is still in its infancy, and many domains remain in various stages of development and refinement. Thus, further efforts are needed to firmly establish DECT as the default technique for CT image acquisition. Second, the use of DECT is limited in morbidly obese patients because of high image noise often interfering with structural and functional image analysis. Third, the image noise of a virtual non-enhanced image is one of the inherent limitations of DECT so that tiny calcifications can be missed. Fourth, larger image datasets with DECT (80/100 kVp, 140 kVp, and average weighted virtual 120 kVp and related material- and energy-specific images) require increased data storage capabilities and appropriate adjustment of clinical workflows.

Conclusions

DECT can provide helpful information for the characterization and staging of thoracic malignancy by quantitatively measuring iodine enhancement on iodine maps or monochromatic imaging. DECT techniques, such as DECT perfusion and ventilation imaging can provide regional lung perfusion and ventilation status and aid in the preoperative prediction of postoperative pulmonary function. Most available data suggest that DECT techniques are radiation-dose neutral compared with conventional single-energy CT examinations. If VNC images from DECT acquisition are routinely used, radiation dose will be further reduced by obviating the need for routine non-contrast scans. More importantly, the substantial incremental diagnostic gain by use of DECT for lung examinations may obviate the need for additional clinical tests that involve radiation, thus reducing the net exposure of the individual patient.

Conflict of interest

UJS is a consultant for and receives research support from Bayer, Bracco, General Electric, Medrad, and Siemens. The other authors have no conflicts of interest to disclose.

References

[1] Nair A, Klusmann MJ, Jogeesvaran KH, Grubnic S, Green SJ, Vlahos I. Revisions to the TNM staging of non-small cell lung cancer: rationale, clinicoradiologic implications, and persistent limitations. Radiographics 2011; 31: 215–238. doi:10.1148/rg.311105039. PMid:21257943.

[2] Sieren JC, Ohno Y, Koyama H, Sugimura K, McLennan G. Recent technological and application developments in computed tomography and magnetic resonance imaging for improved pulmonary nodule detection and lung cancer staging. J Magn Reson Imaging 2010; 32: 1353–1369. doi:10.1002/jmri.22383. PMid:21105140.

[3] Kaza RK, Platt JF, Megibow AJ. Dual-energy CT of the urinary tract. Abdom Imaging 2013; 38: 167–179. doi:10.1007/s00261-012-9901-7. PMid:22581234.

[4] Hartman R, Kawashima A, Takahashi N, et al. Applications of dual-energy CT in urologic imaging: an update. Radiol Clin North Am 2012; 50: 191–205. doi:10.1016/j.rcl.2012.02.007. PMid:22498438.

[5] Kaza RK, Platt JF, Cohan RH, Caoili EM, Al-Hawary MM, Wasnik A. Dual-energy CT with single- and dual-source scanners: current applications in evaluating the genitourinary tract. Radiographics 2012; 32: 353–369. doi:10.1148/rg.322115065. PMid:22411937.

[6] Ko JP, Brandman S, Stember J, Naidich DP. Dual-energy computed tomography: concepts, performance, and thoracic applications. J Thorac Imaging 2012; 27: 7–22. doi:10.1097/RTI.0b013e31823fe0e9. PMid:22189245.

[7] Coursey CA, Nelson RC, Boll DT, et al. Dual-energy multidetector CT: how does it work, what can it tell us, and when can we use it in abdominopelvic imaging? Radiographics 2010; 30: 1037–1055. doi:10.1148/rg.304095175. PMid:20631367.

[8] Yeh BM, Shepherd JA, Wang ZJ, Teh HS, Hartman RP, Prevrhal S. Dual-energy and low-kVp CT in the abdomen. AJR Am J Roentgenol 2009; 193: 47–54. doi:10.2214/AJR.09.2592. PMid:19542394.

[9] Kim KS, Lee JM, Kim SH, et al. Image fusion in dual energy computed tomography for detection of hypervascular liver hepatocellular carcinoma: phantom and preliminary studies. Invest Radiol 2010; 45: 149–157. doi:10.1097/RLI.0b013e3181d32119. PMid:20142749.

[10] Paul J, Bauer RW, Maentele W, Vogl TJ. Image fusion in dual energy computed tomography for detection of various anatomic structures–effect on contrast enhancement, contrast-to-noise ratio, signal-to-noise ratio and image quality. Eur J Radiol 2011; 80: 612–619. doi:10.1016/j.ejrad.2011.02.023. PMid:21376494.

[11] Zhang LJ, Peng J, Wu SY, et al. Liver virtual non-enhanced CT with dual-source, dual-energy CT: a preliminary study. Eur Radiol 2010; 20: 2257–2264. doi:10.1007/s00330-010-1778-7. PMid:20393717.

[12] Silva AC, Morse BG, Hara AK, Paden RG, Hongo N, Pavlicek W. Dual-energy (spectral) CT: applications in abdominal imaging. Radiographics 2011; 31: 1031–1046. doi:10.1148/rg.314105159. PMid:21768237.

[13] Zhou C, Zhao YE, Luo S, et al. Monoenergetic imaging of dual-energy CT reduces artifacts from implanted metal orthopedic devices in patients with factures. Acad Radiol 2011; 18: 1252–1257. doi:10.1016/j.acra.2011.05.009. PMid:21893293.

[14] Li M, Zheng X, Li J, et al. Dual-energy computed tomography imaging of thyroid nodule specimens: comparison with pathologic findings. Invest Radiol 2012; 47: 58–64. doi:10.1097/RLI.0b013e318229fef3. PMid:21788907.

[15] Pisani P, Bray F, Parkin DM. Estimates of the world-wide prevalence of cancer for 25 sites in the adult population. Int J Cancer 2002; 97: 72–81. doi:10.1002/ijc.1571. PMid:11774246.

[16] Chae EJ, Song JW, Seo JB, Krauss B, Jang YM, Song KS. Clinical utility of dual-energy CT in the evaluation of solitary pulmonary nodules: initial experience. Radiology 2008; 249: 671–681. doi:10.1148/radiol.2492071956. PMid:18796658.

[17] Schmid-Bindert G, Henzler T, Chu TQ, et al. Functional imaging of lung cancer using dual energy CT: how does iodine related attenuation correlate with standardized uptake value of ^{18}FDG-PET-CT? Eur Radiol 2012; 22: 93–103. doi:10.1007/s00330-011-2230-3. PMid:21822784.

[18] Chae EJ, Song JW, Krauss B, et al. Dual-energy computed tomography characterization of solitary pulmonary nodules. J Thorac Imaging 2010; 25: 301–310. doi:10.1097/RTI.0b013e3181e16232. PMid:21042068.

[19] Hansell DM, Bankier AA, MacMahon H, McLoud TC, Muller NL, Remy J. Fleischner Society: glossary of terms for thoracic imaging. Radiology 2008; 246: 697–722. doi:10.1148/radiol.2462070712. PMid:18195376.

[20] Guedj N, Couvelard A, Arcangeli G, et al. Angiogenesis and extracellular matrix remodelling in bronchioloalveolar carcinomas: distinctive patterns inmucinous and non-mucinous tumours. Histopathology 2004; 44: 251–256. doi:10.1111/j.1365-2559.2004.01803.x. PMid:14987229.

[21] Uehara T, Honda T, Sano K, et al. A three-dimensional analysis of blood vessels in bronchioloalveolar carcinoma. Lung 2004; 182: 343–353. doi:10.1007/s00408-004-2515-2. PMid:15765926.

[22] Kawai T, Shibamoto Y, Hara M, Arakawa T, Nagai K, Ohashi K. Can dual-energy CT evaluate contrast enhancement of ground-glass attenuation? Phantom and preliminary clinical studies. Acad Radiol 2011; 18: 682–689. doi:10.1016/j.acra.2010.12.014. PMid:21393031.

[23] Goo JM, Park CM, Lee HJ. Ground-glass nodules on chest CT as imaging biomarkers in the management of lung adenocarcinoma. AJR Am J Roentgenol 2011; 196: 533–543. doi:10.2214/AJR.10.5813. PMid:21343494.

[24] Ogawa M, Hara M, Imafuji A, et al. Dual-energy CT can evaluate both hilar and mediastinal lymph nodes and lesion vascularity with a single scan at 60 seconds after contrast medium injection. Acad Radiol 2012; 19: 1003–1010. doi:10.1016/j.acra.2012.03.024. PMid:22621917.

[25] Zhang LJ, Chai X, Wu SY, et al. Detection of pulmonary embolism by dual energy CT: correlation with perfusion scintigraphy and histopathological findings in rabbits. Eur Radiol 2009; 19: 2844–2854. doi:10.1007/s00330-009-1518-z. PMid:19657658.

[26] Zhang LJ, Yang GF, Zhao YE, Zhou CS, Lu GM. Detection of pulmonary embolism using dual-energy computed tomography and correlation with cardiovascular measurements: a preliminary study. Acta Radiol 2009; 50: 892–901. doi:10.1080/02841850903095393. PMid:19639470.

[27] Zhang LJ, Lu GM. Takayasu arteritis involving in pulmonary arteries: evaluation by quantitative dual energy CT pulmonary angiography. Eur Heart J 2012; 33: 928. doi:10.1093/eurheartj/ehr335. PMid:21896563.

[28] Boroto K, Remy-Jardin M, Flohr T, et al. Thoracic applications of dual-source CT technology. Eur J Radiol 2008; 68: 375–384. doi:10.1016/j.ejrad.2008.08.016. PMid:18929452.

[29] Zhang LJ, Zhao YE, Wu SY, et al. Detection of pulmonary embolism by dual energy CT: an experimental study in rabbits. Radiology 2009; 242: 61–70.

[30] Hoey ET, Gopalan D, Screaton NJ. Dual-energy CT pulmonary angiography: a new horizon in the imaging of acute pulmonary thromboembolism. AJR Am J Roentgenol 2009; 192: W341–342. doi:10.2214/AJR.08.1964. PMid:19457800.

[31] Zhang LJ, Wang ZJ, Lu L, Chen B, Lu GM. Feasibility of gadolinium-enhanced dual energy CT pulmonary angiography: a pilot

study in rabbits. Int J Cardiovasc Imaging 2011; 27: 1069–1080. doi:10.1007/s10554-010-9755-4. PMid:21110099.

[32] Goo HW, Yang DH, Kim N, Park SI, Kim DK, Kim EA. Collateral ventilation to congenital hyperlucent lung lesions assessed on xenon-enhanced dynamic dual-energy CT: an initial experience. Korean J Radiol 2011; 12: 25–33. doi:10.3348/kjr.2011.12.1.25. PMid:21228937.

[33] Goo HW, Yang DH, Hong SJ, et al. Xenon ventilation CT using dual-source and dual-energy technique in children with bronchiolitis obliterans: correlation of xenon and CT density values with pulmonary function test results. Pediatr Radiol 2010; 40: 1490–1497. doi:10.1007/s00247-010-1645-3. PMid:20411254.

[34] Thieme SF, Hoegl S, Nikolaou K, et al. Pulmonary ventilation and perfusion imaging with dual-energy CT. Eur Radiol 2010; 20: 2882–2889. doi:10.1007/s00330-010-1866-8. PMid:20571800.

[35] Pontana F, Faivre JB, Remy-Jardin M, et al. Lung perfusion with dual-energy multidetector-row CT (MDCT): feasibility for the evaluation of acute pulmonary embolism in 117 consecutive patients. Acad Radiol 2008; 15: 1494–1504. doi:10.1016/j.acra.2008.05.018. PMid:19000866.

[36] Zhang LJ, Wang ZJ, Zhou CS, Lu L, Luo S, Lu GM. Evaluation of pulmonary embolism in pediatric patients with nephrotic syndrome with dual energy CT pulmonary angiography. Acad Radiol 2012; 19: 341–348. doi:10.1016/j.acra.2011.11.002. PMid:22177283.

[37] Victoria T, Mong A, Altes T, et al. Evaluation of pulmonary embolism in a pediatric population with high clinical suspicion. Pediatr Radiol 2009; 39: 35–41. doi:10.1007/s00247-008-1037-0. PMid:19005649.

[38] Kritsaneepaiboon S, Lee EY, Zurakowski D, Strauss KJ, Boiselle PM. MDCT pulmonary angiography evaluation of pulmonary embolism in children. AJR Am J Roentgen 2009; 192: 1246–1252. doi:10.2214/AJR.08.1299.

[39] Kang DK, Schoepf UJ, Bastarrika G, Nance JW, Jr. Abro JA, Ruzsics B. Dual-energy computed tomography for integrative imaging of coronary artery disease: principles and clinical applications. Semin Ultrasound CT MR 2010; 31: 276–291. doi:10.1053/j.sult.2010.05.004. PMid:20691928.

[40] Zhang LJ, Peng J, Wu SY, Yeh BM, Zhou CS, Lu GM. Dual source dual-energy computed tomography of acute myocardial infarction: correlation with histopathologic findings in a canine model. Invest Radiol 2010; 45: 290–297. PMid:20421797.

[41] Kim SJ, Lim HK, Lee HY, et al. Dual-energy CT in the evaluation of intracerebral hemorrhage of unknown origin: differentiation between tumor bleeding and pure hemorrhage. AJNR Am J Neuroradiol 2012; 33: 865–872. doi:10.3174/ajnr.A2890. PMid:22241388.